Table of Contents

S1. Examples of application of the SAR for elementary and total rate coefficients

S1.1 H-migration in 2,5-dimethylhexylperoxy

In the experiments of Nozière and Vereecken (2019), 2,5-dimethylhexane reacted with Cl atoms in an O_2-containing atmosphere, allowing H-migration in the RO_2 radicals formed. The following steps illustrate how to use the SAR for such aliphatic systems.

The reaction of 2,5-dimethylhexane + Cl + O_2 forms three different peroxy radicals (primary, secondary, and tertiary), which each can undergo between 3 and 5 H-migrations of spans 1,5 or longer (see Nozière and Vereecken, 2019). In the table below, the 298 K rate coefficients for H-migration steps of 2,5-dimethyl-1-hexylperoxy are predicted based on the SAR. Note that the SAR predicts rate coefficients for the entire subgroup, not a per-hydrogen rate. For the 1,8-H-migration, shifting a hydrogen from the remote methyl groups, the final rate coefficient must account for the two indistinguishable $–CH_3$ groups (see table). The calculated total rate coefficient is k_{tot}(298 K) = 2.0×10^{-2} s^{-1}, which is near-exclusively 1,7-H-migration of the tertiary H-atom.

RO_2 reactant	**$HOOQO_2$ product**	**SAR lookup and *k*(298 K)**
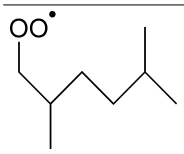	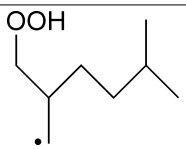	Table 1, 1,5-H-migration Substitution pattern H-atom: $–CH_3$ Substitution pattern $OO^•$: $–CH_2OO^•$ *k*(298 K): 8.22×10^{-6} s^{-1}
	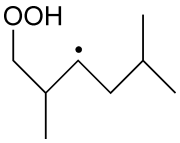	Table 1, 1,5-H-migration Substitution pattern H-atom: $–CH_2–$ Substitution pattern $OO^•$: $–CH_2OO^•$ *k*(298 K): 8.10×10^{-4} s^{-1}
	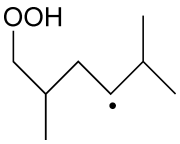	Table 1, 1,6-H-migration Substitution pattern H-atom: $–CH_2–$ Substitution pattern $OO^•$: $–CH_2OO^•$ *k*(298 K): 8.83×10^{-4} s^{-1}
	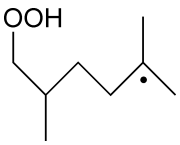	Table 1, 1,7-H-migration Substitution pattern H-atom: –CH< Substitution pattern $OO^•$: $–CH_2OO^•$ *k*(298 K): 1.86×10^{-2} s^{-1}
	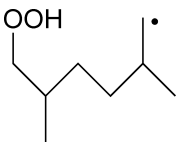	Table 1, 1,8-H-migration Substitution pattern H-atom: $–CH_3$ Substitution pattern $OO^•$: $–CH_2OO^•$ 2 indistinguishable methyl groups *k*(298 K): $2\times 8.60\times10^{-8}$ s^{-1} = 1.72×10^{-7} s^{-1}

Reference

Nozière, B. and Vereecken, L.: Direct Observation of Aliphatic Peroxy Radical Autoxidation and Water Effects: an Experimental and Theoretical Study, Angew. Chem. Int. Ed., DOI: 10.1002/anie.201907981, doi:10.1002/anie.201907981, 2019.

S1.2 H-migration in unsaturated RO_2 radicals

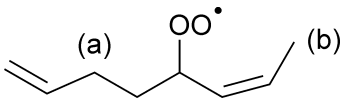

The molecule above has two potential H-migration pathways, a 1,5-H-shift and a 1,6-H-shift. All other H-atoms are either vinylic H-atoms, or at an H-migration span of 1,4 or shorter, and their migration is too slow to contribute.

For migration of the H-atoms on site (a), an allylic radical site is formed, where the double bond is outside the TS ring, requiring use of Table 3. The migration span is a 1,5-H-shift, where the substitution of the H-atom is =C–CH_2–, and that of the peroxy radical site is >CHOO•, leading to a k(298 K) of 2.58×10^{-2} s^{-1}. The other unsaturated bond is not affecting this analysis, and this second branch only changes the substitution pattern on the peroxy group.

For migration of the H-atoms on site (b), an allylic radical site is formed, where the double bond is inside the TS ring, requiring use of Table 2. The migration span is a 1,6-H-shift, where the subsitution of the H-atom is =C–CH_3, and that of the peroxy radical site is >CHOO•, where again the other unsaturation is not affecting the rate beyond counting as a substituent on the peroxy radical base. We thus find a k(298 K) = 1.55×10^{-2} s^{-1}.

The total rate coefficient is then the sum of these group-specific rate coefficients, i.e. k_{tot}(298 K) = 4.1×10^{-2} s^{-1}, with a 62:38 ratio of the two channels.

S1.3 H-migration in multi-functionalized RO_2 radicals

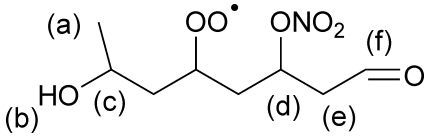

The molecule above has 6 H-atoms at a span of 1,5 or larger; the remaining aliphatic H-atoms have H-migrations spans of 1,4 or shorter, and don't contribute appreciably.

(a) is an aliphatic 1,6-H-migration with a $–CH_3$ and a >CHOO• group, for which Table 1 reports an aliphatic reference k(298 K) rate coefficient of 1.28×10^{-5} s^{-1}. The migrating H-atoms have a β-OH substituent, for which Table 5 shows a 298 K correction factor of 0.16 on the aliphatic rate coefficient, which combined with the earlier rate coefficient predicts a SAR rate coefficient for the (a)-H-atoms of k(298 K) = 2.05×10^{-6} s^{-1}.

(b) is the 1,6-migration of a hydroxyl H-atom by a >CHOO• group. As discussed in section 3.4.3, these reactions are slow, and furthermore the reverse reaction (–OOH H-abstraction by an alkoxy radical –O•) are very fast, such that even if the reaction occurs, the expected fate is reversal of the reaction. Hence, this channel can be neglected.

(c) is the 1,5-H-migration of the carbon-bonded –CHOH– hydrogen atom, for which Table 6 yields k(298 K) = 9.55×10^{-2} s^{-1} when accounting for the >CHOO• group.

(d) corresponds to the 1,5-H-migration of an α-ONO_2 H-atom. Table 5 shows a correction of a factor 4.1×10^{-2} relative to the corresponding aliphatic H-migration, with applicable –CH< and >CHOO• SAR groups, for which Table 1 yield a reference rate coefficient of k(298 K) = 5.80×10^{-2} s^{-1}. After applying the correction, we find a SAR prediction for this H-atom of k(298 K) = 2.4×10^{-3} s^{-1}.

(e) is a 1,6-H-migration of an aliphatic H-atom, with a β-oxo substituent that is outside the TS ring, for which Table 5 prescribes using an aliphatic reference rate coefficient with a 1,6 exo-β-oxo correction at 298 K of 10. The reference rate coefficient from Table 1, using $–CH_2–$ and >CHOO• SAR groups, is k(298 K) = 7.83×10^{-4} s^{-1}, such that the SAR rate coefficient for these H-atoms is k(298 K) = 7.83×10^{-3} s^{-1}. There are no correction factors available for the β-ONO_2 substituent, so this is treated as an aliphatic group for which no correction is needed.

(f) corresponds to a 1,7-H-migration of an aldehydic H-atom by a >CHOO• group, for which Table 4 provides k(298 K) = 1.71×10^{-1} s^{-1}.

This peroxy radical will thus decay by H-migration at a total rate of k(298 K) = 2.8×10^{-1} s^{-1}, of which migration of the α-OH and the aldehydic H-atoms contribute 35 and 62 %, respectively, and are the only channels that would reasonably be included in an atmopsheric chemistry model.

S2. Additional information on methodologies

S2.1 Software

The quantum chemical calculations were performed using the following software suites:

Frisch, M. J., Trucks, G. W., Schlegel, H. B., Scuseria, G. E., Robb, M. A., Cheeseman, J. R., Scalmani, G., Barone, V., Mennucci, B., Petersson, G. A., Nakatsuji, H., Caricato, M., Li, X., Hratchian, H. P., Izmaylov, A. F., Bloino, J., Zheng, G., Sonnenberg, J. L., Hada, M., Ehara, M., Toyota, K., Fukuda, R., Hasegawa, J., Ishida, M., Nakajima, T., Honda, Y., Kitao, O., Nakai, H., Vreven, T., Montgomery Jr., J. A., Peralta, J. E., Ogliaro, F., Bearpark, M., Heyd, J. J., Brothers, E., Kudin, K. N., Staroverov, V. N., Keith, T., Kobayashi, R., Normand, J., Normand, J., Raghavachari, K., Rendell, A., Burant, J. C., Iyengar, S. S., Tomasi, J., Cossi, M., Rega, N., Millam, J. M., Klene, M., Knox, J. E., Cross, J. B., Bakken, V., Adamo, C., Jaramillo, J., Gomperts, R., Stratmann, R. E., Yazyev, O., Austin, A. J., Cammi, R., Pomelli, C., Ochterski, J. W., Martin, R. L., Morokuma, K., Zakrzewski, V. G., Voth, G. A., Salvador, P., Dannenberg, J. J., Dapprich, S., Daniels, A. D., Farkas, O., Foresman, J. B., Ortiz, J. V., Cioslowski, J., Fox, D. J. and Pople, J. A.: Gaussian 09, Revision B.01, Gaussian Inc., Wallington CT., 2010.

Frisch, M. J., Trucks, G. W., Schlegel, H. B., Scuseria, G. E., Robb, M. A., Cheeseman, J. R., Scalmani, G., Barone, V., Mennucci, B., Petersson, G. A., Nakatsuji, H., Li, X., Caricato, M., Marenich, A. V., Bloino, J., Janesko, B. G., Gomperts, R., Mennucci, B., Hratchian, H. P., Ortiz, J. V., Izmaylov, A. F., Sonnenberg, J. L., Williams-Young, D., Ding, F., Lipparini, F., Egidi, F., Goings, J., Peng, B., Petrone, A., Henderson, T., Ranasinghe, D., Zakrzewski, V. G., Gao, J., Rega, N., Zheng, G., Liang, W., Hada, M., Eara, M., Toyota, K., Fukuda, R., Hasegawa, J., Ishida, M., Nakajima, T., Honda, Y., Kitao, O., Nakai, H., Vreven, T., Throssell, K., Mntgomery, Jr., J. A., Peralta, J. E., Ogliaro, F., Bearpark, M. J., Heyd, J. J., Brothers, E. N., Kudin, K. N., Staroverov, V. N., Keith, T. A., Kobayashi, R., Normand, J., Raghavachari, K., Rendell, A. P., Burant, J. C., Iyengar, S. S., Tomasi, J., Cossi, M., Millam, J. M., Klene, M., Adamo, C., Cammi, R., Ochterski, J. W., Martin, R. L., Morokuma, K., Farkas, O., Foresman, J. B. and Fox, D. J.: Gaussian 16, Revision B.01, Gaussian Inc., Wallington CT., 2016.

S2.2 Quantum chemical methodologies for geometry optimization

The following quantum chemical methodologies were used to optimize geometries and calculate vibrational frequencies:

M05-2X/6-311G(d,p)
M05-2X/6-311+G(2df,2p)
M05-2X/aux-cc-pVDZ
M05-2X/aux-cc-pVTZ
M06-2X/6-311+G(2df,2p)
M06-2X/cc-pVDZ
M06-2X/cc-pVTZ
M06-2X/aug-cc-pVTZ
M06-2X-D3/aug-cc-pVTZ
M06-2X/aug-cc-pVQZ
B3LYP/6-31G(d,p) 5 d-orbitals
B3LYP/6-31+G(d,p) 6 d-orbitals
B3LYP/6-31G(2df,p) 6 d-orbitals (used in G3X/G3SX calculations)
B3LYP/6-311G(d,p)
B3LYP/6-311G(2d,d,p) (used in CBS-QB3)
B3LYP/6-311+G(2d,p) 5 d-orbitals
B3LYP/aug-cc-pVDZ

B3LYP/aug-cc-pVTZ
QCISD/6-311G(d,p) (used in CBS-APNO)

Of this list we preferentially use a limited set, to reduce methodological differences somewhat. The most commonly used level of theory is B3LYP/6-31G(d,p) with 5 d-orbitals, M05-2X/6-311G(d,p), and M06-2X/aug-cc-pVTZ. The most accurate of these is the latter methodology, which is used in our recent rate coefficient calculations; the conformers are typically optimized first at the M06-2X/cc-pVDZ level of theory, and re-optimized using the larger basis set.

S2.3 Quantum chemical methodologies used in single-point energy calculations

In addition to the energy information obtained at the same level as the geometry optimization, single point energy calculations are performed at the following levels of theory to obtain more accurate energies:

G3X
G3SX
CBS-QB3
CBS-APNO
CCSD(T)/6-31+G(d') (used in CBS-QB3 calculations)
CCSD(T)/6-311G(d,p)
CCSD(T)/6-311G(2d,p)
CCSD(T)/aug-cc-pVDZ
CCSD(T)/aug-cc-pVTZ
CCSD(T)/aug-cc-pVQZ
QCISD(T)/6-311++G(2df,p) (used in CBS-APNO calculations)
QCISD(T)/6-31G(d) (used in G3X, G3SX calculations)

S2.4 Complete basis set (CBS) energy calculations

We performed CCSD(T) calculations extrapolated to the complete basis set (CBS); these calculations use aug-cc-pVxZ (x = D, T, Q) basis sets, using the aug-Schwartz4(DT) and aug-Schwartz6(DTQ) extrapolation scheme as described by Martin et al. (1996). Table 1 below lists a set of CCSD(T)/CBS barrier heights compared to the barrier height used in the SAR development. The methodology indicated are the level of theory used for the geometry, and the basis sets used in the CBS extrapolation (2 or 3 basis sets using the 'x' values described above). The CBS data are not used in the derivation of the SAR, but they give an idea of how sensitive the barrier heights are to the level of theory. All in all, CBS extrapolations reduce the uncertainty by a few tenths of a kcal mol^{-1} on the barrier height, and are thus able to reduce methodological scatter on the *k*(298 K) rate coefficients by a factor 1.5 to 2. As such, they appear to be less rewarding for the computational cost, considering the uncertainties on e.g. the tunneling corrections and the IRCMax calculations (see below).

Reference

Martin, J. M. L.: Ab initio total atomization energies of small molecules — towards the basis set limit, Chem. Phys. Lett., 259(5–6), 669–678, doi:10.1016/0009-2614(96)00898-6, 1996.

Methodology:

A : M05-2X/6-311G(d,p)
B : B3LYP/6-31G(d,p)
C : M05-2X/aug-cc-pVDZ
D : M05-2X/aug-cc-pVTZ
E : B3LYP/6-31+G(d,p)
F : B3LYP/aug-cc-pVDZ

Table 1: Comparison between the barrier heights (kcal mol^{-1}) used in the kinetic calculations, and improved CCSD(T)/ CBS calculations.

Reactant	**Product**	**E_b (used)**	**E_b (CBS)**	**Meth.**
$^{\bullet}OOCH_2$-CH_2-CH_3	$HOOCH_2$-CH_2-$C^{\bullet}H_2$	25.3	25.29 (DTQ)	A
			24.57 (DT)	B
Z-$^{\bullet}OOCH_2$-CH=C(CH_3)-CH_2OH	Z-$HOOCH_2$-CH=C(CH_3)-$C^{\bullet}HOH$	19.38	19.28 (DT)	A
			19.30 (DT)	C
			19.45 (DT)	D
			19.47 (DT)	E
			19.49 (DT)	F
$^{\bullet}OOCH(CH_3)$-CH_2-CH_2-CHOH-CH_3	$HOOCH(CH_3)$-CH_2-CH_2-$C^{\bullet}OH$-CH_3	16.88	16.88 (DT)	A
$HOCH_2$-CH($OO^{\bullet}$)-CH=O	$HOCH_2$-CH(OOH)-$C^{\bullet}$=O	20.99	20.82 (DT)	A
$HOCH_2$-C(CH_3)($OO^{\bullet}$)-CH=O	$HOCH_2$-C(CH_3)(OOH)-$C^{\bullet}$=O	20.54	20.38 (DT)	A
$^{\bullet}OOCH_2$-C(O)OH	$HOOCH_2$-C(O)$O^{\bullet}$ → OH+CH_2O+CO_2	19.98	20.00 (DTQ)	A
$HOCH_2$-C(CH_3)($OO^{\bullet}$)-C=O(OH)	$HOCH_2$-C(CH_3)(OOH)-C(O)$O^{\bullet}$ → …	19.36	18.72 (DT)	A
$^{\bullet}OOCH_2$-CH_2-CH_2-CH_3	$HOOCH_2$-CH_2-$C^{\bullet}H$-CH_3	22.78	22.61 (DT)	A

S2.5 IRCMax calculations

Some of the quantum chemical methodologies are prone to yielding transition state geometries that are positioned not at the true transition state saddle point, but some (small) distance away, likely towards the products or reactants. This leads to erroneous reaction activation energies. Performing higher-level single point energy calculations on these geometries does not alleviate the problem. IRCMax calculations (Malick et al. 1998) can partially address this problem by performing a series of calculations along the IRC (intrinsic reaction coordinate) trajectory near the TS geometry, and locating the highest energy point along this lower-energy path; this energy maximum is a better estimate of the TS barrier height that would have been obtained by re-optimizing the geometry at the higher level of theory. The method is not able to correct for geometry distortions that are not along the IRC path.

We have performed a series of IRCMax calculations to probe the sensitivity of our predictions to this problem. In Table 2 below we list the energy difference between a higher-level single point energy calculations at the transition state geometry obtained using a lower level of theory, and the highest energy obtained at that higher-level methodology when calculation additional points along the IRC path. We find that B3LYP-based transition state geometries differ strongly from those at higher levels of theory, leading to errors on the energy calculations of up to a kcal mol^{-1}; these geometries thus add an additional uncertainty of up to a factor 5 on the predicted k(298 K) rate coefficients. M05-2X and M06-2X geometries are much more reliable, and are generally at or very near the optimal IRCMax geometry, inducing errors of 20% or less on the k(298 K) values. As the training and test data sets for the SAR extensively use B3LYP geometries, the resulting increased scatter introduces additional uncertainty on the SAR predictions. The only solution is to redo all calculations at a higher level of theory, avoiding B3LYP-based data in the SAR.

Reference

Malick, D. K., Petersson, G. A. and Montgomery, J. A.: Transition states for chemical reactions I. Geometry and classical barrier height, J. Chem. Phys., 108(14), 5704–5713, doi:10.1063/1.476317, 1998.

Table 2: IRCMax calculations for a set of methodologies, listing the difference between the TS geometry energy and the IRCMax energy (kcal mol^{-1})

Reactant	Product	Methodology	ΔE
$^{\bullet}OOCH_2$-CH_2-CH_3	$HOOCH_2$-CH_2-$C^{\bullet}H_2$	CBS-QB3//B3LYP/CBSB7	0.22
		CBS-QB3//M05-2X/6-311G(d,p)	0.00
		CBS-APNO//M05-2X/6-311G(d,p)	0.00
		CCSD(T)/aug-cc-pVDZ//M05-2X/6-311G(d,p)	0.00
$^{\bullet}OOCH_2$-CH_2-CH_2-CH_3	$HOOCH_2$-CH_2-$C^{\bullet}H$-CH_3	CBS-QB3//B3LYP/CBSB7	0.24
$^{\bullet}OOCH_2$-CH_2-$CH(CH_3)$-CH_3	$HOOCH_2$-CH_2-$C^{\bullet}(CH_3)$-CH_3	CBS-QB3//B3LYP/CBSB7	0.26
		CBS-QB3//M05-2X/6-311G(d,p)	0.00
$^{\bullet}OOCH_2$-CH=CH-CH_3	$HOOCH_2$-CH=CH-$C^{\bullet}H_2$	CBS-QB3//B3LYP/CBSB7	0.11
		CBS-QB3//B3LYP/6-31+G(d,p)	0.08
		CBS-QB3//M05-2X/6-311G(d,p)	0.00
Z-$^{\bullet}OOCH_2$-CH=$C(CH_3)$-CH_2OH	Z-$HOOCH_2$-CH=$C(CH_3)$-$C^{\bullet}HOH$	CBS-QB3//B3LYP/6-31+G(d,p)	0.69
		CBS-APNO//B3LYP/6-31+G(d,p)	0.19
		G3SX//B3LYP/6-31G(2df,p)	0.11
		CBS-QB3//M05-2X/6-311G(d,p)	0.03
		CBS-APNO//M05-2X/6-311G(d,p)	0.00
Z-$^{\bullet}OOCH_2$-$C(CH_3)$=CH-CH_2OH	Z-$HOOCH_2$-$C(CH_3)$=CH-$C^{\bullet}HOH$	CBS-QB3//B3LYP/6-31+G(d,p)	0.47
		G3SX//B3LYP/6-31G(2df,p)	0.10
		CBS-QB3//M05-2X/6-311G(d,p)	0.00
		CBS-APNO//M05-2X/6-311G(d,p)	0.01
$^{\bullet}OOCH(CH_3)$-CH_2-CH_2-CH_2OH	$HOOC(CH_3)$-CH_2-CH_2-$C^{\bullet}HOH$	CBS-QB3//B3LYP/CBSB7	0.39
		CBS-QB3//B3LYP/6-31+G(d,p)	0.45
		CBS-QB3//M05-2X/6-311G(d,p)	0.00
		CBS-APNO//M05-2X/6-311G(d,p)	0.04
$HOCH_2$-$CH(OO^{\bullet})$-CH=O	$HOCH_2$-CH(OOH)-$C^{\bullet}$=O	CBS-QB3//B3LYP/CBSB7	1.04
		CBS-QB3//B3LYP/6-31G(2df,p)	1.01
		G3SX//B3LYP/6-31G(2df,p)	0.43
		CBS-QB3//M05-2X/6-311G(d,p)	0.13
		CCSD(T)/aug-cc-pVDZ//M05-2X/6-311G(d,p)	0.12
		CCSD(T)/aug-cc-pVTZ//M05-2X/6-311G(d,p)	0.06
$HOCH_2$-$C(CH_3)(OO^{\bullet})$-CH=O	$HOCH_2$-$C(CH_3)$(OOH)-$C^{\bullet}$=O	CBS-QB3//B3LYP/CBSB7	1.12
		CBS-QB3//M05-2X/6-311G(d,p)	0.17
		CCSD(T)/aug-cc-pVDZ//M05-2X/6-311G(d,p)	0.12
		CBS-APNO//M05-2X/6-311G(d,p)	0.06
$^{\bullet}OOCH_2$-C(O)OH	$HOOCH_2$-C(O)$O^{\bullet}$ →	G3SX//B3LYP/6-31G(2df,p)	2.40
	CO_2 + OH + HCHO	CBS-QB3//M05-2X/6-311G(d,p)	0.00
		CCSD(T)/aug-cc-pVDZ//M05-2X/6-311G(d,p)	0.00
		CCSD(T)/aug-cc-pVTZ//M05-2X/6-311G(d,p)	0.00
		CBS-APNO//M05-2X/6-311G(d,p)	0.08

S2.6 Relative multi-conformer transition state theory (rel-MC-TST)

Relative multi-conformer transition state theory (rel-MC-TST) leverages MC-TST (Vereecken and Peeters, 2003) rate coefficients calculation on a reference reaction to obtain estimates of rate coefficients of "similar" reactions relative to the reference reaction at a reduced cost. The required quantum chemical calculations are all conformers for the MC-TST rate coefficient of the reference calculation, and a small set of additional calculations on selected conformers of the target reaction. A formal derivation, and benchmarking, will be published in an upcoming publication; we limit ourselves here to a brief outline of the approach, and provide a minimum number of equations.

S2.6.1 Brief outline of rel-MC-TST

The rate of any target reaction can be written as a temperature-dependent ratio $R(T)$ between the rate coefficient of a reference reaction and that of the target reaction;

$$k_{target}(T) = k_{ref}(T)\, x\, R(T) \qquad \text{(E.S1)}$$

MC-TST expresses a rate coefficient in a transition state paradigm, explicitly summing the contributions of the reactant(s) and transition state (TS) conformers by their respective partition functions:

$$k(T) = \frac{kT}{h} \times \frac{\sum_i \kappa_i(T) Q_i^{\neq}(T) \exp\left(\frac{-E_i}{kT}\right)}{\sum_i Q_A^i(T) \exp\left(\frac{-E_i}{kT}\right)} \times \exp\left(\frac{-E_b}{kT}\right) \qquad \text{(E.S2)}$$

where $Q_i(T)$ indicates the partition function (usually in a rigid rotor harmonic oscillator approximation) for conformer i at temperature T (A signifies the reactant, $\neq$ is the TS with exclusion of the reaction coordinate mode), E_i the conformer ZPE-corrected energy relative to the lowest conformer, E_b the energy difference between the energetically lowest conformers of reactant and transition state; k is the Boltzmann constant and h Plank's constant. κ_i is the tunneling correction; typically, this correction is taken identical for all conformers, e.g. an Eckart tunneling correction for the lowest conformer.

The ratio $R(T)$ can be expressed as a ratio of partition functions and Boltzmann-weighted reaction energies for the reference and target reaction, which in turn can be compacted to a ratio of rate coefficients:

$$\begin{aligned} k_{target}(T) &= k_{ref}(T) x \left(\frac{\sum_i \kappa^i_{target}(T) Q^{\neq,i}_{target}(T) \exp\left(\frac{-E^i_{target}}{kT}\right)}{\sum_i \kappa^i_{ref}(T) Q^{\neq,i}_{ref}(T) \exp\left(\frac{-E^i_{ref}}{kT}\right)} \right) \times \left(\frac{\sum_i Q^{A,i}_{ref}(T) \exp\left(\frac{-E^i_{ref}}{kT}\right)}{\sum_i Q^{A,i}_{target}(T) \exp\left(\frac{-E^i_{target}}{kT}\right)} \right) \times \exp\left(\frac{-\left(E^b_{target} - E^b_{ref}\right)}{kT}\right) \\ &= k_{ref}(T) x \frac{k_{target}(T)}{k_{ref}(T)} \end{aligned} \qquad \text{(E.S3)}$$

which is trivially true if the ratio is calculated using all conformers (full MC-TST) for both reactions. Relative MC-TST consists of approximating the ratio by using only a selected set of conformers for reactant and transition states:

$$k_{target}(T) = k_{ref}(T) x \frac{k^{selected}_{target}(T)}{k^{selected}_{ref}(T)} \qquad \text{(E.S4)}$$

where the approximation becomes better as more conformers are included in the selection, up to the limit of including all conformers. In the ratio, one uses a similar (limited) number and type of conformers for both the reference and target reaction. Essentially, this approach samples the ratio of entropy and energy of corresponding reactant and transition state conformers between reference and target reaction, and the difference in reaction barrier height that implies. In as much as the average change in molecular structure is represented in the properties of the selected conformers, this provides an estimate of the target rate coefficient without having to calculate all conformers of the target reaction. Furthermore, given that some conformers have a larger contribution to the populations, or are more representative for the molecular change between reference and target reaction, a judicious choice of conformers led by chemical

knowledge can lead to rapid convergence of the ratio. A good selection will thus choose conformers that contribute strongly, choose conformers in reference and target reaction that correspond as well as possible, choose conformers that represent the change in molecular structure between reference and target best (e.g. absence/presence of H-bonding), and choose the included number of conformers in reference and target to correct for changes in number of total conformers (e.g. changes in number of internal rotors due to a new double bond in the target molecule). In the extreme limit, even a single, well-chosen conformer each for reactant and TS can be sufficient to obtain a fair estimate of the ratio.

S2.6.2 Benefits of rel-MC-TST

A key benefit of rel-MC-TST is that the selection of the conformers is guided by the information from the MC-TST analysis of the reference reaction, based on information on all conformers. Intrinsically, the target rate coefficient is then indirectly based on information on all conformers, through the ratios of properties; this ratio is often similar across many/most conformers. The selection of the most representative conformers, and generating starting geometries for the modified molecular structure of the target conformers, benefits greatly from the full-conformer information available from the analysis of the reference reaction. Aided with some chemical knowledge, one can then readily characterize a small selection of conformers of the target reaction and calculate the rate ratio with fair confidence. Rel-MC-TST is particularly useful for theoretical work aimed at structure-activity relationships, as there one performs a systematic set of changes on a base molecular structure. It is also useful for the theoretical characterization of reaction mechanisms; examples include the study of isoprene or terpenoid oxidation mechanisms, which often involve similar molecules undergoing similar reactions, changing only in the positioning of the (spectator) substituents.

Møller et al. (2016) have described an approximation to MC-TST to reduce the computational cost, implemented by generating about half of all conformers at a semi-empirical level of theory rather than attempting a near-exhaustive characterization of the full population using a quantum chemical wave function or DFT method; from this subset of conformers, higher-level calculations are then performed on those conformers contributing most to the population. As discussed briefly by Novelli et al. (2020), the proposed conformer selection process based on semi-empirical methods does not reliably generate the most contributing conformers, leading to a larger *a priori* uncertainty of 1 to 2 orders of magnitude, though the method yields good results if the reaction studied is amenable to cancellation of error, which is often the case. An earlier implementation (Zhang and Dibble, 2011) using semi-empirical methods to generate conformers, was likewise found to miss important conformers. Compared to conformer sampling by semi-empirical methods, the rel-MC-TST technique described here is more robust even with a small selection of conformers, as full-conformer information from the reference reaction is readily used to ensure the best possible estimate for the least amount of effort, with only a minimal risk of unknown omissions. It is also more cost-effective, as one does not need to generate conformers from scratch for each reaction. Indeed, a single (costly) MC-TST reference rate coefficient can be used to affordably generate estimates for many target reaction rate coefficients. The current study, for example, uses the four 1-hexylperoxy H-migrations (spans 1,5 through 1,8) as a reference for 27 reactions. Finally, the set of conformers included in the rel-MC-TST calculation can be systematically enlarged, characterizing additional conformers for the target reaction until convergence is obtained, thus allowing balancing computational cost versus accuracy.

As all relative techniques, rel-MC-TST works best if the target reaction is as comparable as possible to the reference reaction. A suitable MC-TST reference reaction may not be available, precluding efficient application of the technique by still requiring the characterization of a large fraction of the target conformers. In these cases, it is best to treat one reaction in a set of similar target reactions as a new reference reaction, and characterize it first by MC-TST. Rel-MC-TST is also likely to work best for molecules of comparable number of conformers, as adding additional internal rotors (and hence combinatorially increasing the number of conformers) may make it difficult to find corresponding sets of conformers in target and reference reaction. Finally, while the technique can be applied as a black-box method, it is more efficient to use chemical knowledge to select conformers, taking into account changes in steric hindrance, H-bonding, and other molecular variations.

S2.6.3 Application of rel-MC-TST in the current work

Section 3 lists a set of rate coefficients derived using rel-MC-TST, and the rate coefficient they are based on. Although we do not describe benchmarks of rel-MC-TST at this time, we find that the rate coefficients for which we have target $k(T)$ values, the rate coefficients predicted by rel-MC-TST usually fit well within the SAR framework. In a few cases,

deviations of over 1 order of magnitude are suspected. However, we have applied rel-MC-TST in an extreme way, using 1 to 6 conformers only, truly a bare minimum. The overall good performance is a good indicator of the robustness of the method. A future paper benchmarking the approximation will make recommendations regarding the number of conformers to use, and how to select the most representative conformers.

References

Møller, K. H., Otkjær, R. V., Hyttinen, N., Kurtén, T. and Kjaergaard, H. G.: Cost-Effective Implementation of Multiconformer Transition State Theory for Peroxy Radical Hydrogen Shift Reactions, J. Phys. Chem. A, 120(51), 10072–10087, doi:10.1021/acs.jpca.6b09370, 2016.

Novelli, A., Vereecken, L., Bohn, B., Dorn, H.-P., Gkatzelis, G. I., Hofzumahaus, A., Holland, F., Reimer, D., Rohrer, F., Rosanka, S., Taraborrelli, D., Tillmann, R., Wegener, R., Yu, Z., Kiendler-Scharr, A., Wahner, A. and Fuchs, H.: Importance of isomerization reactions for the OH radical regeneration from the photo-oxidation of isoprene investigated in the atmospheric simulation chamber SAPHIR, Atmospheric Chem. Phys., 20, 3333–3355, doi:acp-20-3333-2020, 2020.

Vereecken, L. and Peeters, J.: The 1,5-H-shift in 1-butoxy: A case study in the rigorous implementation of transition state theory for a multirotamer system, J. Chem. Phys., 119(10), 5159–5170, doi:10.1063/1.1597479, 2003.

Zhang, F. and Dibble, T. S.: Effects of Olefin Group and Its Position on the Kinetics for Intramolecular H-Shift and HO_2 Elimination of Alkenyl Peroxy Radicals, J. Phys. Chem. A, 115(5), 655–663, doi:10.1021/jp1111839, 2011.

S3. Absolute rate coefficient predictions

All rate coefficients in this section are calculcated using MC-TST, incorporating all conformers.

Methodologies:

A	CCSD(T)/aug-cc-pVTZ//M06-2X-D3/aug-cc-pVTZ
B	CCSD(T)/aug-cc-pVTZ//M06-2X/aug-cc-pVTZ
C	CBS-APNO//B3LYP/6-31G(d,p)
D	CCSD(T)/aug-cc-pVTZ//M05-2X/6-311G(d,p)
E	CBS-QB3//B3LYP/6-31G(d,p)
F	CBS-APNO//M05-2X/6-311G(d,p)
G	CBS-QB3//M05-2X/6-311G(d,p)
H	CCSD(T)/CBS//M06-2X-aug-cc-pVTZ
I	G3SX

Reactant	**Span**	**Subst. OO / H**	**Method**	***k*(298 K) / s^{-1}**	***A* / s^{-1}**	***n***	***E*$_a$ / K**
$^{\bullet}$OO-CH$_2$-CH$_2$-CH$_3$	1,5	1° / 1°	A	6.04×10^{-6}	6.20E-34	14.32	5108
$^{\bullet}$OO-CH$_2$-CH$_2$-CH$_2$-CH$_3$	1,6	1° / 1°	B*	2.76×10^{-4}	4.84E-22	10.46	5565
$^{\bullet}$OO-CH$_2$-CH$_2$-CH$_2$-CH$_2$-CH$_3$	1,5	1° / 2°	B*	4.39×10^{-4}	2.27E-20	9.91	5654
	1,6	1° / 2°	B*	6.58×10^{-4}	1.15E-14	7.85	5941
	1,7	1° / 1°	B*	3.82×10^{-6}	2.02E-16	8.16	6806
CH$_3$-CH$_2$(OO$^{\bullet}$)-CH$_2$-CH$_2$-CH$_3$	1,5	2° / 2°	B*	1.01×10^{-3}	8.68E-19	9.46	5718
	1,6	2° / 1°	B*	8.81×10^{-6}	7.28E-16	8.31	7183
$^{\bullet}$OO-CH$_2$-CH$_2$-CH(CH$_3$)-CH$_3$	1,5	1° / 3°	C	2.87×10^{-2}	1.39E-02	4	6572
$^{\bullet}$OO-CH$_2$-CH$_2$-CH$_2$-CH$_2$-CH$_2$-CH$_3$	1,5	1° / 2°	B*	5.93×10^{-4}	1.97E-19	9.61	5690
	1,6	1° / 2°	B*	9.50×10^{-4}	1.38E-13	7.51	5990
	1,7	1° / 2°	B*	3.43×10^{-4}	1.10E-18	8.91	5172

	1,8	1° / 1°	B*	4.92×10^{-8}	4.73E-25	10.7	6489
•OO-CH_2-CH_2-CH_2-CH(CH_3)-CH_3	1,6	1° / 3°	D	2.19×10^{-2}	1.67E-03	4.27	6482
•OO-CH_2-CH_2-CH_2-CH_2-CH(CH_3)-CH_3	1,7	1° / 3°	E	2.43×10^{-1}	5.58E-11	6.53	4472
•OO-CH_2-CH(CH_3)-CH_2-CH_2-CH(CH_3)-CH_3	1,5	1° / 1°	B	7.86×10^{-6}	1.64E-31	13.55	5381
	1,5	1° / 2°	B	4.00×10^{-3}	6.89E-40	16.23	2326
	1,6	1° / 2°	B	5.99×10^{-3}	1.59E-27	12.04	3576
	1,7	1° / 3°	B	5.76×10^{-2}	1.07E-41	16.28	375
	1,8	1° / 1°	B	1.48×10^{-7}	3.20E-29	12.1	5678
CH_3-C(CH_3)(OO•)-CH_2-CH_2-CH(CH_3)-CH_3	1,5	3° / 2°	B	1.38×10^{-3}	1.00E-29	13.06	4235
	1,6	3° / 3°	B	8.94×10^{-2}	1.28E-35	14.71	1747
	1,7	3° / 1°	B	2.47×10^{-5}	4.57E-25	10.98	5094
CH_3-CH(CH_3)-CH(OO•)-CH_2-CH(CH_3)-CH_3	1,5	2° / 1°	B	3.96×10^{-5}	1.31E-27	12.46	5719
	1,5	2° / 3°	B	9.02×10^{-2}	1.64E-35	14.99	2286
	1,6	2° / 1°	B	5.55×10^{-5}	6.75E-29	12.73	5196
Z-•OO-CH=CH-CH_2-CH_3	1,5	2° / 2° endo-=	E	9.24×10^{-2}	2.30E-76	28.7	-2469
Z-•OO-CH_2-CH=CH-CH_3	1,6	1° / 2° endo-=	E	2.17×10^{-2}	3.94E-75	27.57	-3115
Z-•OO-C(CH_3)=CH-CH_3	1,5	2° / 1° endo-=	E	2.95×10^{-3}	1.02E-89	33.22	-2935
Z-•OO-CH=C(CH_3)-CH_3	1,5	2° / 1° endo-=	E	4.24×10^{-4}	1.91E-95	35.01	-3246
Z-•OO-CH_2-CH=CH-CH_2-CH_3	1,6	1° / 2° endo-=	E	6.38×10^{-1}	2.29E-69	25.74	-3268
Z-•OO-CH_2-CH_2-CH=CH-CH_3	1,7	1° / 2° endo-=	E	1.18×10^{0}	8.54E-60	22.36	-2615
•OO-CH_2-CH_2-CH_2-CH=CH_2	1,5	1° / 2° exo-=	E	1.69×10^{0}	4.43E-63	23.77	-2595
Z-•OO-CH=CH-CH(CH_3)-CH_3	1,5	2° / 3° endo-=	E	8.57×10^{-1}	7.44E-68	25.98	-1906
Z-•OO-CH_2-C(CH_3)=CH-CH_3	1,6	1° / 1° endo-=	E	4.05×10^{-2}	5.49E-75	27.56	-3219
Z-•OO-CH_2-CH_2-CH_2-CH=CH-CH_3	1,5	1° / 2° exo-=	E	1.88×10^{0}	8.20E-62	23.31	-2529

E-•OO-CH_2-CH_2-CH_2-CH=CH-CH_3	1,5	1° / 2° exo-=	E	2.30×10^{0}	1.54E-61	23.31	-2410
•OO-CH_2-CH_2-CH_2-CH_2-CH=CH_2	1,6	1° / 2° exo-=	E	3.12×10^{0}	1.88E-56	21.38	-2277
Z-•OO-CH_2-CH=CH-CH(CH_3)-CH_3	1,6	1° / 3° endo-=	E	1.35×10^{1}	1.20E-56	21.76	-2204
Z-•OO-CH_2-CH_2-CH_2-CH_2-CH=CH-CH_3	1,6	1° / 2° exo-=	E	6.21×10^{0}	6.97E-53	20.19	-2064
E-•OO-CH_2-CH_2-CH_2-CH_2-CH=CH-CH_3	1,6	1° / 2° exo-=	E	3.90×10^{0}	4.68E-55	20.96	-2104
•OO-CH_2-CH_2-CH_2-CH_2-CH_2-CH=CH_2	1,7	1° / 2° exo-=	E	7.16×10^{0}	7.85E-56	21.15	-2497
•OO-$CH(CH_3)$-CH-CH_2-CH_2-CH_2OH	1,6	2° / 2°(OH)	E	1.19×10^{0}	3.54E+08	0.5	6665
•OO-$CH(CH_3)$-CH-CH_2-CH_2-CH(OH)-CH_3	1,6	2° / 3°(OH)	E	5.50×10^{-1}	2.51E-01	3.42	5577
•OO-CH_2-CH_2-CH=O	1,5	1° / 3°(=O)	E	4.84×10^{0}	1.96E-39	16.21	492
			C	9.74×10^{0}	3.66E-37	15.46	573
•OO-CH_2-CH_2-CH_2-CH=O	1,6	1° / 3°(=O)	E	4.94×10^{0}	2.03E-41	16.79	101
•OO-CH_2-CH_2-CH_2-CH_2-CH=O	1,7	1° / 3°(=O)	E	1.83×10^{0}	2.91E-30	12.9	1458
(R,R) O=CH-C(CH_3)(OO•)-CH(OOH)-CH_2(OOH)	1,4	3° / 3°(=O)	B*	1.15×10^{0}	1.21E-83	30.69	-4811
	1,4	3° / 3°(OOH)	B*	4.88×10^{-3}	4.59E-82	28.94	-3276
	1,5	3° / 2°(OOH)	B*	1.18×10^{-5}	2.87E-35	15.11	3586
	1,6	3° / OOH	B*	1.84×10^{4}	7.26E-40	15.39	-3656
	1,7	3° / OOH	B*	6.29×10^{4}	2.75E-25	10.85	-1725
(R,R) O=CH-C(CH_3)(OOH)-CH(OO•)-CH_2(OOH)	1,5	2° / 3°(=O)	B*	3.34×10^{1}	1.12E-67	25.15	-4273
	1,6	2° / OOH (primary)	B*	1.88×10^{4}	1.17E-34	13.27	-3683
	1,6	2° / OOH (tertiary)	B*	2.97×10^{4}	1.36E-38	14.73	-4035
(R,R) O=CH-C(CH_3)(OOH)-CH(OOH)-CH_2(OO•)	1,6	1° / 3°(=O)	B*	2.28×10^{0}	3.57E-41	16.93	788
	1,6	1° / OOH	B*	2.35×10^{3}	3.06E-33	13.03	-2486
	1,7	1° / OOH	B*	1.27×10^{4}	1.35E-22	9.96	-906
(R,S) O=CH-C(CH_3)(OO•)-CH(OOH)-CH_2(OOH)	1,4	3° / 3°(=O)	B*	3.71×10^{0}	7.07E-75	27.88	-3914

	1,4	3° / 3°(OOH)	B*	8.44×10^{-5}	2.52E-68	24.59	-1817
	1,5	3° / 2°(OOH)	B*	5.02×10^{-2}	8.69E-27	12.33	3989
	1,6	3° / OOH	B*	6.34×10^{4}	7.94E-17	7.46	-1680
	1,7	3° / OOH	B*	6.20×10^{4}	4.02E-20	9.43	-579
(R,S) O=CH-C(CH_3)(OOH)-CH($OO^{\bullet}$)-CH_2(OOH)	1,5	2° / 3°(=O)	B*	3.05×10^{-1}	4.28E-75	28.3	-2589
	1,6	2° / OOH (primary)	B*	1.32×10^{3}	4.40E-22	9.34	-926
	1,6	2° / OOH (tertiary)	B*	2.07×10^{3}	7.58E-19	7.91	-1277
(R,S) O=CH-C(CH_3)(OOH)-CH(OOH)-CH_2($OO^{\bullet}$)	1,6	1° / 3°(=O)	B*	4.86×10^{1}	6.99E-37	15.2	-133
	1,6	1° / OOH	B*	9.89×10^{3}	7.65E-28	11.39	-1308
	1,7	1° / OOH	B*	1.52×10^{3}	6.68E-28	11.93	-558
$^{\bullet}$OO-CH_2-C(=O)OH	1,5	1° / COOH	D	3.10×10^{-1}	2.42E-68	26.07	-1799
			I	3.42×10^{-2}	3.45E+08	1.05	8647
$^{\bullet}$OO-CH(CH_3)-C(=O)OH	1,5	2° / COOH	I	1.38×10^{0}	1.44E+08	1.16	7472
CH_2(OH)-C(CH_3)($OO^{\bullet}$)-C(=O)OH	1,5	3° / COOH	D	1.60×10^{0}	3.73E-54	21.18	-842
Z-$^{\bullet}$OO-CH_2-CH=C(CH_3)-CH_2(ONO_2)	1,6	1° / 2°(ONO_2) endo-=	B	1.90×10^{-2}	7.72E-78	28.02	-4158
E-$^{\bullet}$OO-CH_2-CH=C(CH_2ONO_2)-CH_3	1,6	1° / 1° endo-=	B	1.48×10^{-3}	2.58E-84	30.21	-4128
$^{\bullet}$OO-C(CH_3)(-CH=CH_2)-CH_2(ONO_2)	1,4	3° / 2°(ONO_2)	B	1.84×10^{-8}	8.78E-73	26.48	827
	1,4	3° / 1°	B	1.55×10^{-10}	4.82E-75	27.35	2170
Z-$^{\bullet}$OO-CH_2-C(CH_3)=CH-CH_2(ONO_2)	1,6	1° / 2°(ONO_2) endo-=	B	5.35×10^{-2}	2.52E-75	27.06	-4374
	1,5	1° / 1° gem-=	B	3.28×10^{-4}	1.07E-96	34.33	-5178
E-$^{\bullet}$OO-CH_2-C(CH_3)=CH-CH_2(ONO_2)	1,6	1° / 2°(ONO_2) endo-=	B	4.81×10^{-4}	2.94E-97	34.68	-5088
CH_2(ONO_2)-CH($OO^{\bullet}$)-C(=CH_2)-CH_3	1,5	1° / 1° gem-=	B	8.51×10^{-4}	5.58E-89	32.05	-4050
$^{\bullet}$OO-CH_2-C(ONO_2)(-CH=CH_2)-CH_3	1,5	1° / 1°	B	8.93×10^{-6}	6.45E-40	16.3	4235
$^{\bullet}$OO-CH_2-CH(ONO_2)-C(=CH_2)-CH_3	1,6	1° / 1° gem-=	B	1.72×10^{-2}	8.97E-67	24.55	-2426

CH_3-CH_2($OO^{\bullet}$)-CH_2-CH_2-CH_2(OOH)	1,5	2° / 2°	B*	4.41×10^{-4}	1.90E-35	14.77	3553
	1,6	2° / 2°(OOH)	B*	8.44×10^{-3}	3.77E-40	15.89	1341
	1,8	2° / OOH	B*	1.17×10^{2}	9.14E-15	6.76	423
$^{\bullet}OO$-CH_2-CH_2-CH_2-CH(OOH)-CH_3	1,5	1° / 2°	B*	3.95×10^{-4}	2.68E-38	15.73	3249
	1,6	1° / 3°(OOH)	B*	1.84×10^{-1}	1.07E-64	23.93	-2761
	1,7	1° / 1°	B*	3.18×10^{-7}	1.18E-12	6.96	8093
	1,8	1° / OOH	B*	4.14×10^{2}	3.48E-25	10.16	-1327
CH_2(OH)-CH($OO^{\bullet}$)-CH=O	1,4	2° / 3°(=O)	F	1.42×10^{0}	1.88E-54	21.22	-947
			G	3.38×10^{-1}	2.31E-59	22.83	-1157
			D	3.97×10^{-2}	1.08E-66	25.23	-1470
CH_2(OH)-C(CH_3)($OO^{\bullet}$)-CH=O	1,4	3° / 3°(=O)	D	1.40×10^{-1}	2.54E-63	24.25	-1193
	1,5	3° / OH	D	1.32×10^{-6}	9.32E+12	-0.61	11904
	1,4	3° / 2°(OH)	D	6.07×10^{-6}	3.24E-44	17.66	3717
CH_2(OH)-CH($OO^{\bullet}$)-C(=O)-CH_3	1,5	1° / 1°(endo-β=O)	D	4.94×10^{-5}	2.94E+15	-1.35	11283
			H	3.84×10^{-5}	2.05E-57	21.74	1083
	1,4	2° / 2°(OH)	H	3.19×10^{-5}	3.11E-81	29.64	-1790
	1,5	2° / OH	H	877×10^{-5}	7.13E+11	-0.24	10571
$^{\bullet}OO$-CH_2-CH(OH)-C(=O)-CH_3	1,5	1° / OH	H	4.95×10^{-4}	1.25E+11	-0.03	9897
	1,4	1° / 3°(OH)	H	1.46×10^{-2}	5.87E-80	28.33	-4988
	1,6	1° / 1°(endo-β=O)	H	1.44×10^{-3}	1.13E-35	14.61	2828
7-hydroxy-1-menthenyl-8-peroxy	1,5	cyclic	E	4.60×10^{-5}	6.74E-03	3.9	8104
	1,6	cyclic	E	4.24×10^{-5}	7.72E-46	17.86	-1061
2-hydroxy-1-menthenyl-8-peroxy	1,6	cyclic	E	4.16×10^{-3}	6.99E-10	6.43	6275
pinonaldehydeperoxy	1,5	cyclic	E	8.70×10^{-5}	3.17E-70	25.97	-815

	1,8	cyclic	E	3.66×10^{-6}	7.65E-76	27.42	-1264
	1,9	cyclic	E	2.07×10^{-3}	8.31E-49	18.83	808
1-hydroxymenthyl-2-oxa-3,3-diMe-bicyclo[2.2.2]octane-syn-6-peroxy	1,5	cyclic	E	3.96×10^{-5}	1.18E+06	1.92	7018
1-hydroxymenthyl-2-oxa-3,3-diMe-bicyclo[2.2.2]octane-anti-6-peroxy	1,5	cyclic	E	8.60×10^{-2}	7.75E-06	5.59	6710
$^{\bullet}OOCH_2(OH)$	1,3	1° / 2°(OH)	B	3.89×10^{-13}	4.81E-199	69.16	-10187
	1,4	1° / OH	B	1.84×10^{3}	1.17E+11	0.45	6127
$^{\bullet}OOCH(OH)_2$	1,4	2° / OH	B	6.73×10^{7}	7.93E+04	2.37	2018

* published in Novelli et al. (2019) ; Fuchs et al. (2018) ; Nozière and Vereecken (2019) ;

S4. Relative rate coefficient predictions

All quantum chemical calculations are performed at the B3LYP/6-31G(d,p) (5 d-orbitals) level of theory. All rate coefficients in this section are calculcated using rel-MC-TST, incorporating only a handful of conformers.

Reference molecules:

A	1-hexylperoxy
B	1-OH-4-pentylperoxy
C	1-butene-1-peroxy
D	2-pentene-1-peroxy
E	3-pentene-1-peroxy
F	4-pentene-1-peroxy
G	5-hexene-1-peroxy
H	6-heptene-1-peroxy

Reactant	Span	Subst. OO / H	Ref. Reaction	k(298 K) / s^{-1}	A / s^{-1}	n	E_a / K
•OO-CH_2-CH_2-CH_2-CH_2-CH_2-CH_2-CH_3	1,5	1° / 2°	A	4.55×10^{-4}	2.22E+02	2.84	8719
	1,6	1° / 2°	A	1.33×10^{-3}	4.53E+06	1.31	8770
	1,7	1° / 2°	A	1.65×10^{-3}	1.43E+09	0.27	8643
	1,8	1° / 2°	A	1.31×10^{-5}	7.76E-01	3.02	8396
•OO-CH_2-CH(OH)-CH_2-CH_2-CH_2-CH_2-CH_3	1,5	1° / 2°(β-OH)	A	8.83×10^{-5}	2.62E+02	2.91	9380
•OO-CH_2-C(=O)-CH_2-CH_2-CH_2-CH_2-CH_3	1,5	1° / 2°(endo-β=O)	A	1.79×10^{-4}	4.23E-74	27.41	-1251
	1,6	1° / 2°	A	9.86×10^{-5}	7.79E-19	9.39	6267
•OO-CH_2-CH_2-CH(CH_3)-CH_2-CH_2-CH_2-CH_3	1,5	1° / 3°	A	4.55×10^{-2}	2.75E-04	4.75	6539
•OO-CH_2-CH_2-CH(OH)-CH_2-CH_2-CH_2-CH_3	1,5	1° / 3°(OH)	A	6.10×10^{-1}	5.54E-02	4.12	6277
	1,6	1° / 2°(β-OH)	A	3.07×10^{-4}	4.34E+03	2.24	8702
•OO-CH_2-CH_2-C(=O)-CH_2-CH_2-CH_2-CH_3	1,6	1° / 2°(endo-β=O)	A	7.61×10^{-3}	1.47E-31	13.27	2825
	1,7	1° / 2°	A	1.03×10^{-5}	4.88E-06	4.89	8075
•OO-CH_2-CH_2-CH_2-CH(CH_3)-CH_2-CH_2-CH_3	1,6	1° / 3°	A	2.16×10^{-2}	7.40E-03	4.11	6651
•OO-CH_2-CH_2-CH_2-CH(OH)-CH_2-CH_2-CH_3	1,5	1° / 2°(β-OH)	A	2.98×10^{-4}	2.86E+12	-0.19	10640
	1,6	1° / 3°(OH)	B	7.58×10^{-1}	7.47E+12	-0.71	7708
	1,7	1° / 2°(β-OH)	A	3.09×10^{-5}	4.65E+08	0.45	9804
•OO-CH_2-CH_2-CH_2-C(=O)-CH_2-CH_2-CH_3	1,5	1° / 2°(exo-β=O)	A	8.81×10^{-2}	7.64E-24	10.92	3402
	1,7	1° / 2°(endo-β=O)	A	3.08×10^{-3}	6.17E-27	11.41	3108
•OO-CH_2-CH_2-CH_2-CH_2-CH(CH_3)-CH_2-CH_3	1,7	1° / 3°	A	1.56×10^{-3}	1.53E-07	5.4	6415
•OO-CH_2-CH_2-CH_2-CH_2-CH(OH)-CH_2-CH_3	1,6	1° / 2°(β-OH)	A	1.37×10^{-4}	1.41E+02	2.69	8693
	1,7	1° / 3°(OH)	A	2.12×10^{-1}	1.17E-01	3.51	5782
•OO-CH_2-CH_2-CH_2-CH_2-C(=O)-CH_2-CH_3	1,5	1° / 2°	A	7.20×10^{-5}	1.32E-03	4.47	8457
	1,6	1° / 2°(exo-β=O)	A	1.99×10^{-2}	4.48E-24	10.8	3484

•OO-CH_2-CH_2-CH_2-CH_2-CH_2-CH(CH_3)-CH_3	1,8	1° / 3°	A	2.53×10^{-8}	1.36E-22	10.11	7367
•OO-CH_2-CH_2-CH_2-CH_2-CH_2-CH(OH)-CH_3	1,7	1° / 2°(β-OH)	A	1.97×10^{-5}	8.05E-08	5.8	8199
•OO-CH_2-CH_2-CH_2-CH_2-CH_2-C(=O)-CH_3	1,6	1° / 2°	A	3.07×10^{-5}	9.50E-04	4.34	8383
	1,7	1° / 2°(endo-β=O)	A	9.43×10^{-3}	9.01E-27	11.59	3187
Z-•OO-CH=CH-CH_2-CH_2-CH_2-CH_2-CH_3	1,5	1° / 2° endo-=	C	5.11×10^{-2}	2.31E-94	34.58	-4675
Z-•OO-CH_2-CH=CH-CH_2-CH_2-CH_2-CH_3	1,6	1° / 2° endo-=	D	1.19×10^{-2}	2.27E-70	26.02	-2292
	1,7	1° / 2°	A	8.53×10^{-5}	2.17E-04	4.6	8081
Z-•OO-CH_2-CH_2-CH=CH-CH_2-CH_2-CH_3	1,7	1° / 2° endo-=	E	3.24×10^{0}	1.83E-44	17.39	-836
Z-•OO-CH_2-CH_2-CH_2-CH=CH-CH_2-CH_3	1,5	1° / 2° exo-=	F	1.43×10^{0}	8.16E-53	20.41	-1195
Z-•OO-CH_2-CH_2-CH_2-CH_2-CH=CH-CH_3	1,6	1° / 2° exo-=	G	6.07×10^{0}	5.42E-44	17.33	-802
Z-•OO-CH_2-CH_2-CH_2-CH_2-CH_2-CH=CH_2	1,7	1° / 2° exo-=	H	5.18×10^{0}	3.18E-43	17.02	-761
Z-•OO-CH_2-CH_2-CH_2-CH_2-CH_2-CH=CH_2-CH_3	1,7	1° / 2° exo-=	H	1.45×10^{1}	3.94E-45	17.68	-1251

S5. Spreadsheet for SAR derivation (FAIR)

In an attempt to make the SAR derivation more FAIR, we provide a spreadsheet that implements the derivation process as described in the main paper; for those that are unable to open the spreadsheet, a PDF version is also provided. For each of the SAR reaction classes, a set of 4 calculation blocks is provided, placed from left to right. The spreadsheet is an exact replication of the SAR derivation for the tables provided in the main text.

S5.1 Literature data

The first block (see figure below) lists the reaction class (in the example below a 1,4-H-migration with a -$CH_2OO^{\bullet}$ peroxy radical and a migrating H-atom from a carbon bearing three hydrogen atoms (-CH_3). For the list of temperatures (column with header "T"), the available rate data is calculated, with indication of the source, and the parameters (P1, P2, P3) used in the kinetic expression, if any.

1,4 Hshift						
	P1	1.26E+12	5.6E+11	5.67E+13		1.00E-02
	P2	16930	0.2	1.88E+04		4.007
	P3		34.2	5.26E+08		12964
-CH2OO. | -CH3	T	Miyoshi 2011	Sharma et al.	Otkjaer et al.	Otkjaer et al.	Zhang and Dibb
	200	2.17E-25	1.71E-26			1.17E-21
	225	2.64E-21	2.49E-22			2.53E-18
	250	4.90E-18	5.34E-19			1.23E-15
	260	6.62E-17	7.60E-18			1.05E-14
	270	7.39E-16	8.90E-17			7.77E-14
	280	6.94E-15	8.73E-16			4.99E-13
	290	5.58E-14	7.32E-15	9.24E-06		2.84E-12
	298	2.67E-13	3.62E-14	9.71E-06	3.72E-11	1.05E-11
	310	2.41E-12	3.42E-13	1.21E-05		6.63E-11
	320	1.33E-11	1.95E-12	1.62E-05		2.78E-10
	330	6.60E-11	1.00E-11			1.07E-09
	340	2.99E-10	4.67E-11			3.84E-09
	350	1.24E-09	1.99E-10			1.28E-08
	375	3.11E-08	5.37E-09			2.00E-07
	400	5.23E-07	9.57E-08			2.25E-06
	425	6.31E-06	1.22E-06			1.93E-05
	450	5.77E-05	1.17E-05			1.32E-04

A similar block is also used when calculating the average temperature dependence, when needed. Instead of kinetic data, the data columns will then contain rate predictions for SAR classes that are deemed useful for obtaining such an average temperature dependence. These blocks are marked with the "Average temperature dependence" title.

S5.2 Selection of target *k*(298 K) and temperature dependence

The second block lists the desired temperature dependence and target *k*(298 K). If enough data of sufficient quality is available, this can be the geometric mean of the selected data. For those cases where not enough data is available to derive a temperature dependence, an average T-dependence will be linked from elsewhere on the sheet; such averaged T-dependencies are marked in red. In many cases, no suitable data is available to derive a *k*(298 K) target value. The target value is then determined by using the averaged ratio between the substituted rates for those reactions where data is available, and the corresponding class for aliphatic peroxy radicals, i.e. the target reaction class will scale similar to the aliphatic RO_2. Such averaged k(298K) targets are marked in orange. Finally, the *T*-dependence and the target k(298K) are merged, resulting in a "Final" rate coefficient curve that goes through the target *k*(298 K) value and has a *T*-dependence scaled to that of the selected *T*-dependence.

A similar block is also used when calculating the average temperature dependence, when needed. The target *k*(298 K) value and the "Final" column are in this case used merely to visualise the data (see below)

		Ea shift
		-1.12E+03
T-dependenc	Target	Final
1.63E-24		4.34E-22
1.18E-20		1.69E-18
1.47E-17		1.28E-15
1.74E-16		1.28E-14
1.72E-15		1.08E-13
1.45E-14		7.79E-13
1.05E-13		4.93E-12
4.67E-13	1.98E-11	1.98E-11
3.79E-12		1.39E-10
1.93E-11		6.32E-10
8.92E-11		2.63E-09
3.77E-10		1.00E-08
1.47E-09		3.56E-08
3.22E-08		6.32E-07
4.83E-07		7.86E-06
5.29E-06		7.31E-05
4.46E-05		5.33E-04

S5.3 Fitting to a (modified) Arrhenius expression

The temperature-dependent rate coefficient derived earlier is then fitted to both an Arrhenius expression $k(T) = A \times \exp(-E_a / T)$ and a modified Arrhenius expression $k(T) = A \times (T/\mathrm{K})^n \times \exp(-E_a / T)$. The parameters are listed in orange, and have units s^{-1} (A factors) and K (E_a factors); n is unit-less. The columns 1000/T, 1/T, log(1/T) and log(k) are used for the fitting procedure and for visualisation.

The goodness of recovery is probed by calculating the rate coefficient at the lowest and highest temperature, and calculating the ratio between the (modified) Arrhenius fit value and the original $k(T)$ curve, to check if these extreme values are correctly replicated. This is given in the column "Replicate", which has an upper block with 4 values for the Arrhenius fit; the top value is k(lowest T), followed by the ratio for that T, and below that the k(highest T) value preceded by the ratio for that T. A similar block of 4 values is listed next to the modified Arrhenius parameters for that fit. The modified Arrhenius expression gives a near-perfect fit in all cases, and is used throughout; the quality of the fit for the traditional Arrhenius expression will depend strongly on the curvature in the Arrhenius plot.

1000/T	1/T	log(1/T)	log(-CH2OO-)	log(T)	Replicate
5.00	5.00E-03	-2.30E+00	-2.14E+01	A	3.97E-22
4.44	4.44E-03	-2.35E+00	-1.78E+01	1.48E+11	0.92
4.00	4.00E-03	-2.40E+00	-1.49E+01	Ea	
3.85	3.85E-03	-2.41E+00	-1.39E+01	1.50E+04	
3.70	3.70E-03	-2.43E+00	-1.30E+01		1.03
3.57	3.57E-03	-2.45E+00	-1.21E+01		8.03E-13
3.45	3.45E-03	-2.46E+00	-1.13E+01	-1.40E+00	
3.36	3.36E-03	-2.47E+00	-1.07E+01	-6.33E+03	
3.23	3.23E-03	-2.49E+00	-9.86E+00	7.08E+00	
3.13	3.13E-03	-2.51E+00	-9.20E+00	#N/A	
3.03	3.03E-03	-2.52E+00	-8.58E+00	#N/A	
2.94	2.94E-03	-2.53E+00	-8.00E+00	A	1.00E-08
2.86	2.86E-03	-2.54E+00	-7.45E+00	1.21E+07	1.00
2.67	2.67E-03	-2.57E+00	-6.20E+00	n	
2.50	2.50E-03	-2.60E+00	-5.10E+00	1.40	
2.35	2.35E-03	-2.63E+00	-4.14E+00	Ea	1.00
2.22	2.22E-03	-2.65E+00	-3.27E+00	14586	5.33E-04

S5.4 Visualisation of the source data and final expression

For those SAR classes where there is literature data available, a plot is shown depicting $k(T)$ / s^{-1} against 1000 K / T. The available literature data is shown, either as a curve or as discrete values depending on the type of source data. The final SAR rate is also depicted as a dotted line.

Average temperature dependencies also have a plot, showing the source data, and the averaged *T*-dependence derived from that data; this serves only to visualize the averaging procedure.

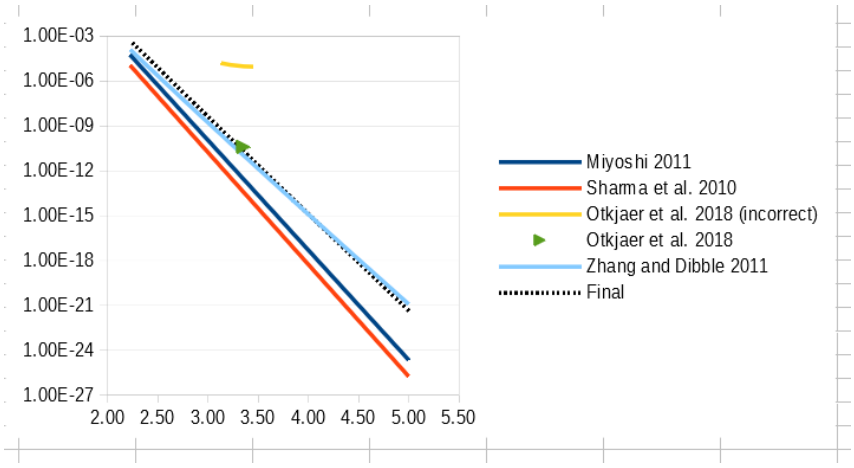

S5.5 Modifying or updating the SAR

The spreadsheet provided allows one to easily change the values used to derived the SAR expression, e.g. by adding data, removing data from the selection, or providing alternative *k*(298 K) target values or *k*(*T*) temperature dependencies. Mostly, this involves only adding the data, and changing the underlying formulas to include / exclude the available data as wanted. No additional add-ins, macros, or scripts are necessary beyond the standard formulas of commonly used spreadsheet programs. The original spreadsheet was developed in Libreoffice, a freely downloadable Office suite.

S6. Transferability of the temperature dependence

For SAR classes where insufficient data is available to determine the temperature dependence of the rate coefficient k(T), the SAR derivation applies the temperature dependence of a similar SAR class. This is only valid if the temperature dependence is transferable between the different reactions. The degree of transferability is illustrated here for two groups of classes.

The first reaction class group shown is 1,4-H-migration in aliphatic RO_2; this group is characterized by high energy barriers and virtually no curvature in the Arrhenius plots.

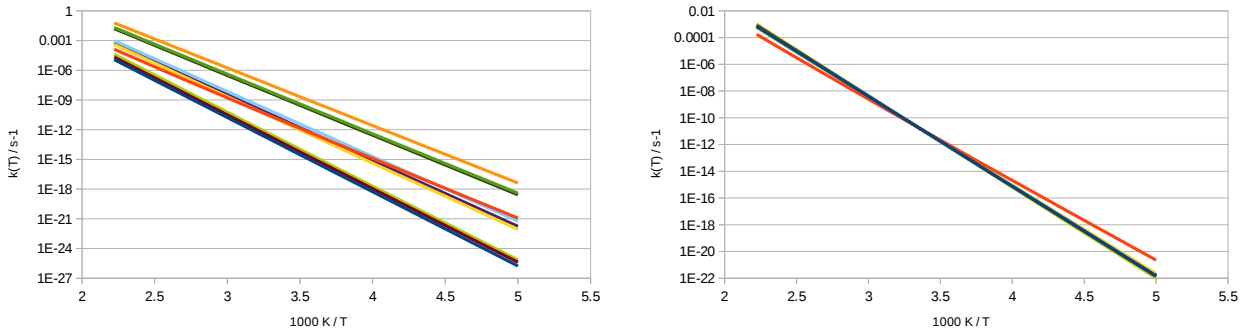

The left-hand side plot shows the available theoretical rate coefficients for all substitution patterns. As can be seen, the rate coefficients differ by 6 orders of magnitude at room temperature. The right-hand side plot shows the same rate coefficients, after shifting the rate coefficients to their geometric average by applying an exp(Corr/T) correction (see main text for details), with a different Corr value for each reaction such that the same target k(298 K) is recovered. It is clear that the resulting curves have excellent overlap, and the shifted temperature-dependence is transferable across all SAR substituent classes. Specifically, an equally good overlap is obtained for any k(298 K) used as the target value for

shiftng the curves. Two slightly different lines are found; the trend difference is due to application of different levels of theoretical methodologies, but the difference is slight, even negligible in the critical 250-350 K temperature range.

A similar set of plots is shown for the aliphatic 1,5-H-migration; this group of reactions is characterized by lower energy barriers, higher rate coefficients, and significant curvature in the Arrhenius plots due to tunneling contributions at the lowest temperatures.

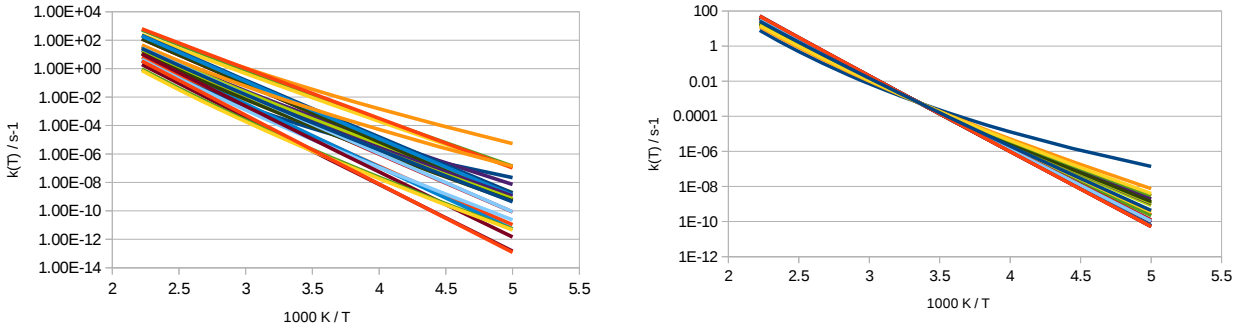

The available theoretical rate coefficients near room temperature (shown in the left-hand side plot) differ by 4 orders of magnitude. The righ-hand side plot shows the same rate coefficients, but each shifted to a common k(298 K) target value using the aforementioned exp(Corr/T) correction factor (see main text). For the temperature range 250-450 K, the curves deviates from the average temperature dependence by only a factor 2 to 3 across all reactions. At low temperatures, down to 200 K, the curves fan out somewhat, as tunneling in this temperature regime becomes more important and even minor reaction difference start to play a prominent role. One reaction class in particular (the 1,5-H-migrations of tertiary >CH– H-atoms to a tertiary >C(OO•)– group) has a somewhat stronger curvature. At these low temperatures, the rates for H-migration are too low to be competitive, and these predictions are less important, but still we see that even there, rate coefficients with transferred *T*-dependenciss should be within a factor of 10 of the averaged *T*-dependence, sufficient to estimate whether the reaction can be important or not. To some extent, this fanning-out of the curves is also a function of the level of theory applied, but mostly due to slight differences in energy, entropy and tunneling. This is illustrated in the plot below, which shows only rate coefficients calculated at the same level of theory. As can be seen, the spread across the curves is somewhat less, but still sizable at 200 K.

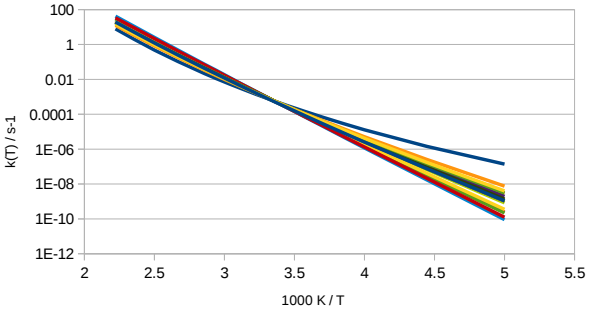

It should be stressed that the graphs shown above show a worst-case scenario. Any temperature-dependence transferred from one SAR class to another is selected such as to be based on those reference classes most comparable to the target class. As such, we estimate that even at the lowest temperatures considered, the uncertainty on the SAR predictions caused by the transfer of temperature-dependence of k(T) between classes is likely of the order of a factor 2 to 4. Near room temperature (250-350 K), this should be a factor of 2 or less. Future theoretical and experimental studies on those reaction classes for which T-dependence transfer was necessary will reveal whether these assessments are accurate.

S7. Raw quantum chemical data

The most important quantum chemical data is provided in a separate text file, showing geometries, moments of inertia, vibrational wavenumbers, and (single point) energies, at all levels of theory where data is available.